JOURNAL OF GEOPHYSICAL RESEARCH, VOL. 98, NO. C2, PAGES 2475–2483, FEBRUARY 15, 1993

Satellite Altimeter Measurements of Surface Wind

ROMAN E. GLAZMAN AND ALEXANDER GREYSUKH

Jet Propulsion Laboratory, California Institute of Technology, Pasadena

Recent analyses of wind speed measurements by the Geosat altimeter showed that the radar cross section is affected by oceanographic factors, particularly by the degree of sea development, which are not directly accounted for in the geophysical model functions (GMF). In the present work, two new GMFs which account for the effects of the actual degree of sea development are proposed. Along with the radar cross section, these models use significant wave height information. One particular version is recommended for applications in oceanographic and climate studies where wind speed (or wind stress) data have to be binned (i.e., averaged over time and/or space intervals). The accuracy of this GMF (overall bias of 0.1 m/s and rms error of about 1.6 m/s) is higher than the accuracy of commonly employed GMFs, while the wave-age-related trend is reduced to a geophysically insignificant level. Finally, the wind speed histograms for the collocated data set are derived and compared with the ground truth data as well as with the histograms yielded by presently known GMFs. It is also shown that the accuracy of altimeter measurements could be increased even further if some additional information on the wave field were available from independent sources (e.g., the dominant wavelength from synthetic aperture radar images).

1. INTRODUCTION

In recent years the influence of sea maturity on satellite measurements received considerable attention: satellite scatterometer, altimeter, and microwave radiometer measurements of surface winds were reexamined (see *Glazman* [1991*a*] for a review) and the sea state bias was investigated on the basis of Geosat altimeter data [*Fu and Glazman*, 1991]. These studies revealed the existence of an error trend which is related to the sea maturity and is present, to a greater or smaller degree, in all satellite microwave measurements. For wind speed measurements by an altimeter, the wave-age-related trend is especially important: it could result in systematic regional distortions of wind fields by more than 2 m/s. In the present work, geophysical model functions (GMFs) which greatly reduce this error trend and improve the overall accuracy of wind speed measurements are proposed. Two fundamentally different approaches are tested, and the approach based on the use of a classifier is recommended as yielding the best results in terms of both the measuring accuracy and the computational efficiency.

The rms ("standard") error of satellite measurements is the most commonly used characteristic of the measuring accuracy. However, depending on the specific application, other characteristics may also be important. For instance, if the wind speed measurements are used to prepare maps of wind stress over the ocean, the absolute mean error becomes highly important. Indeed, the wind stress is usually determined as $\tau = C_D U^2$ where C_D is the drag coefficient. The satellite-reported wind U_S contains random error e: $U_S = U_{true} + e$. Therefore the wind stress is

$$\tau = C_D(U_{true}^2 + 2eU_{true} + e^2) \tag{1}$$

Both the rms error $\langle e^2 \rangle^{1/2}$ and the mean absolute error $\langle e \rangle$ contribute to an error in the estimated wind stress. (The angle brackets denote averaging of the data within appropriate bins.) Equation (1) allows one to formulate the requirements to the accuracy of wind speed measurements in terms of the mean error $\langle e \rangle$. Suppose the lowest rms error achievable by satellite measurements is 1.7 m/s. We shall demand that the mean error $\langle e \rangle$ remain near or below $\langle e^2 \rangle/2U$, which limits the contribution of the second term in the right-hand side (r.h.s.) of (1) to that of the third term. Take $U_{true} \approx 7$ m/s and $\langle e^2 \rangle^{1/2} \approx 1.7$ m/s. Apparently, in order to neglect the contribution of the second term in the r.h.s. of (1) compared with that of the third term, the condition $\langle e \rangle \ll 0.2$ m/s must hold. Thus a requirement that the mean error $\langle e \rangle$ be below 0.2 m/s can be viewed as a criterion of applicability of altimeter (as well as other instruments') wind speeds as input to wind-driven circulation models. With $\langle e \rangle$ as large as 0.5 m/s, the wind stress would be biased by about 15%.

We can also impose a limit on the wave-age-related trend in wind measuring errors. Suppose that this trend can be crudely quantified by a linear function $e = C_0 + C_1\xi$, where ξ is the pseudo wave age (equations (2) and (3) below) and C_1 is the "trend coefficient" in meters per second per unit ξ (see the following sections for more detail). Then if the range of ξ variation within a given region and/or period is about 2, the ξ-related error trend will result in a false trend of about $2C_1$ m/s in the (spatial and/or temporal) distribution of the altimeter-reported wind. Evidently, limiting the value of C_1 to 0.5 m/s per unit ξ reduces this false trend to the level which is well below the random error, while a value of C_1 as high as 1 m/s makes this trend prominent even on the random background.

In section 3 we provide statistical characterization of three currently employed GMFs, and in section 5 we demonstrate that an approximate knowledge of the wave age (based on some auxiliary measurements) could facilitate a dramatic improvement of wind speed measurements, not only in terms of the rms error but also in terms of the mean error and higher-order statistics such as the third-order statistical moment $\langle e^3 \rangle$. The wave age effects could be accounted for on the basis of the dominant wavelength obtainable from synthetic aperture radar (SAR) images, or using collocated-buoy measurements of the dominant wave period. In the absence of such auxiliary information, effects of the wave

Paper number 92JC02659.
0148-0227/93/92JC-02659$05.00

age can still be quantified, and wind speed measurements can be improved, although the task is more difficult. In sections 4–6 the corresponding GMF is developed utilizing information on the significant wave height (SWH) extracted from altimeter wave forms. Although the accuracy gain is not as dramatic as in the case of more reliable, buoy- or SAR-supplied wave information, it leads to a considerable improvement of satellite data and reduces the wave-age-related error bias to an acceptable level.

Sea maturity characterizes the degree of wave development with respect to a given wind. For an intuitive understanding of this notion, consider two extreme situations: a sea arising under a strong local wind of short duration, and a well-developed sea dominated by waves arriving from a remote location, observed at a low local wind. The "young sea" of the first example has a small wave age ξ, where ξ is defined as the ratio of the phase velocity of the dominant waves, C_0, to the mean speed of the local wind, U:

$$\xi = C_0/U \tag{2}$$

The "old" sea of the second example may have very large ξ. A less controversial term for this case is "pseudo wave age," which remains meaningful even when the sea is contaminated by swell [*Fu and Glazman*, 1991]. The wave age was found to influence geometrical properties of the sea surface; hence its remote sensing signature [*Glazman*, 1991*a*]. One of the factors yielding large values of ξ is the weakly nonlinear wave-wave interactions resulting in the growth of long waves (due to a spectral flux of wave action towards low wavenumbers). Such interactions are slow, and they require a large distance for the waves to exchange energy in the course of their propagation. Hence the wind fetch is an important parameter determining the wave age. Other factors include stratification of the marine boundary layer, the wind duration, ambient currents, etc. The notion of the wave age is not free of some controversy [*Pierson*, 1991]. Theoretical background on this topic along with implications of the theory and its use in the context of ocean remote sensing are provided by *Glazman and Weichman*, [1989], *Glazman* [1990, 1991*a*, *b*], and *Glazman and Srokosz* [1991].

As before [*Glazman and Pilorz*, 1990], we shall estimate the wave age based on the buoy-supplied wind speed U_B and significant wave height H_B. To this end, we shall use an empirical relationship

$$\xi = A(gH/U^2)^{2\nu} \tag{3}$$

where $A \approx 3.24$ and $\nu \approx 0.31$. This relationship can be also derived theoretically [*Glazman and Srokosz*, 1991]. A more direct way of estimating the wave age is based on the equation $\xi = g/\omega_0 U$, where ω_0 is the dominant wave frequency. Although these two equations give similar results, (3) has an advantage of being easier to interpret under complex conditions of wave generation, when the dominant wave frequency is difficult to define. Then ξ of (3) should be called more appropriately the "pseudo wave age" [*Fu and Glazman*, 1991]. Equation (3) is especially useful when the wind speed and SWH are the only parameters available from direct measurements. However, the accuracy of (3) drops rapidly as the errors in U increase above a certain level. According to *Gilhousen* [1987], the rms error of wind speed measurements by National Data Buoy Center (NDBC) buoys is within 10% of the wind speed (or 1 m/s, whichever is greater). It can be readily shown that this accuracy corresponds to a 10% error in the determination of ξ by (3) and is comparable to the error of the direct determination based on $\xi = g/\omega_0 U$ (see also *Glazman* [1991*b*] for additional discussion of this issue).

2. COLLOCATED MEASUREMENTS BY NDBC BUOYS AND GEOSAT ALTIMETER

A collocated set of autonomous buoy (of the National Data Buoy Center) and Geosat altimeter measurements for the period November 1986 through July 1989 was compiled at the Jet Propulsion Laboratory (JPL) from Geosat geophysical data record (GDR) and NDBC data. (This data set is presently available through the JPL Physical Oceanography Distributed Active Archive Center.) One-second averages of altimeter measurements were used, which tentatively correspond to footprint spacing of about 7 km. The collocation procedure and characteristics of the data are described by *Glazman and Pilorz* [1990], who employed a 1-year subset of this data set. Being interested only in a special case of equilibrium sea state, Glazman and Pilorz eliminated observations characterized by complex conditions of wave development. The entire data set containing all observations for 2.6 years was employed later by *Glazman* [1991*a*], who found that the error trend discovered earlier under idealized conditions remained prominent under general conditions of wave generation. The data set employed in the present work is slightly smaller than the data set employed by *Glazman* [1991*a*]: we include here only the cases for which the satellite attitude angle ATT did not exceed 0.82°, whereas *Glazman* [1991*a*] included cases with ATT up to 0.85°. The 0.82° had been found earlier [*Glazman and Pilorz*, 1990] as the critical attitude which, if surpassed, leads to an appreciable drop in the quality of Geosat altimeter measurements. Also, the spatial collocation window is only 0.5°, as opposed to 1° in the *Glazman* [1991*a*] study. The temporal collocation window is reduced to 45 min.

For the stage of the algorithm development, the data set was further cleaned in order to increase the reliability of the data. We applied a slight amount of low-pass spatial filtering: a running averaging along the track, covering three consecutive points, was applied to the radar cross section and the significant wave height. Finally, a few obvious outliers were also eliminated. These were defined as points with the radar cross section above 25 dB, below 6 dB, and outside the range of 2.5 times the standard deviation from an empirical curve for $\sigma_0(U)$. Points with SWH exceeding 11 m and those with SWH outside the range of 2.5 standard deviations from the best fit between H_B and H_S were also deleted as outliers. When the development of the GMFs (described below) was completed, we used original unfiltered data to estimate errors and other statistics of our GMFs as well as of the GMFs developed by other authors.

The following buoy measurements were used: wind speed U_B (averaged over an 8.5-min interval), significant wave height H_B (based on the integrated wave spectrum), and anemometer height for each buoy (used to reference all wind speed measurements to the standard height of 10 m). The Geosat altimeter data employed are the radar cross section σ_0, in decibels; the attitude angle of the satellite, ATT, in degrees (to eliminate faulty observations); and the SWH,

H_S, which we corrected using equation (4) below. The wind speed U_S was obtained from σ_0 by means of the Brown GMF [*Brown et al.*, 1981]. Other GMFs were also tested: the modified Chelton-Wentz (tabular) GMF [*Witter and Chelton*, 1991] and the "smoothed" Brown algorithm [*Dobson et al.*, 1987]. For each buoy record (made on hourly or 3-hour basis), we used up to eight (1-s averaged) Geosat observations along the satellite track; the actual number depends on the length of the track segment within the spatial collocation window. The total number of independent buoy measurements retained in the collocated data set was 865. The total number of altimeter data points was 5682, which yields an average of 6.6 altimeter observations per each buoy measurement.

Carter et al. [1992] showed that SWH is systematically underestimated by the Geosat altimeter. To eliminate possible adverse effects of the error trend in the altimeter SWH, we developed a simple empirical algorithm

$$H_S = 0.113 + 1.0278\ H + 0.0124\ H^2 \qquad (4)$$

where H is the SWH from Geosat altimeter original records.

3. ALTIMETER WIND SPEED MEASUREMENTS BASED ON THE RADAR CROSS SECTION

According to *Dobson et al.* [1987], the most accurate GMF for altimeter wind speed is due to *Brown et al.* [1981]. Like other known GMFs, it relates the radar cross section σ_0 to the mean wind U at 10-m height. Earlier [*Glazman and Pilorz*, 1990], the actual relationship between U and σ_0 was found to be ambiguous: at a given wind speed, the observed σ_0 may vary depending on the wave age ξ. Since the influence of ξ is pronounced only at relatively small ξ, we quantify this error trend by means of the coefficient C_1 in the linear regression model: $e = C_0 + C_1\xi$ for the range of ξ from 0 to 4. The trend of the Brown GMF was estimated to be about 0.7 m/s per unit ξ [*Glazman*,1991*a*]. For the present data set, the mean error of the Brown GMF is found to be $\langle e\rangle \approx 0.17$ m/s, the error trend $C_1 \approx 1.0$ m/s per unit ξ, while the rms error is 1.69 m/s (see Table 1 and Figure 1). Therefore if the wave age in two geographic regions differs by 3, the corresponding false difference in wind speed measurements will attain 3 m/s, which is well above the rms error of the Brown GMF. From Figure 1 it is also clear that if the wave-age-related trend could be reduced, it might help decrease the overall rms error as well. Of course, the rms error and the trend coefficient C_1 are not the only important criteria by which to evaluate the performance of the GMFs. Additional criteria are listed in Table 1. Specifically, the absolute mean error $\langle e\rangle$ and the third moment $\langle e^3\rangle$ are important: the former characterizes the overall mean bias (see the discussion in section 1), and the latter quantifies the skewness of the error distribution and is affected by large errors bordering with statistical outliers. In section 7 we discuss histograms of wind speed distributions, which leads us to an additional (more precisely, alternative) constraint on

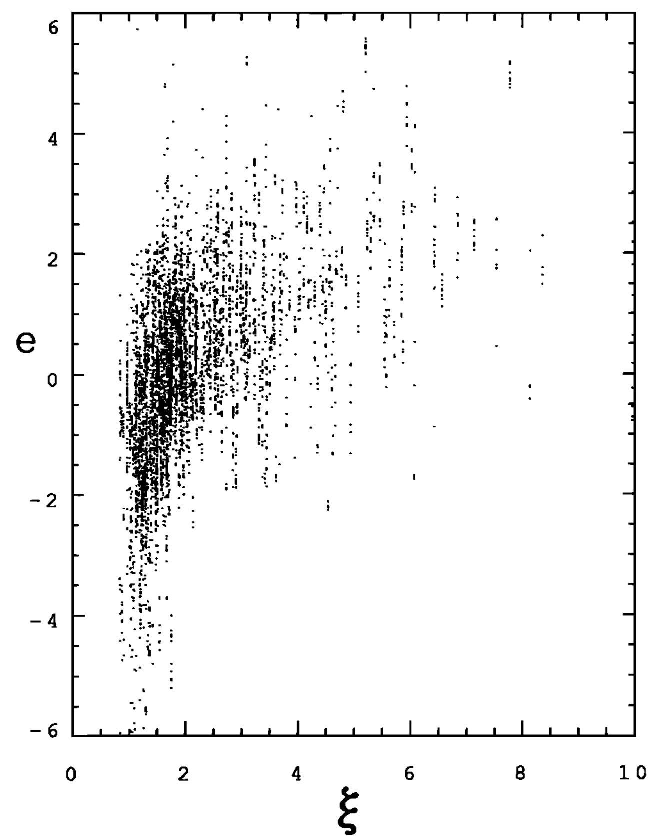

Fig. 1. Wind speed error $e = (U_S - U_B)$, in meters per second, versus pseudo wave age, ξ. The latter is based on buoy data and equation (3). U_S is the altimeter wind speed by the Brown GMF; U_B is the buoy-supplied wind speed.

TABLE 1. Characteristics of GMFs

Wind Speed GMF	Mean Error $\langle e\rangle$, m/s	Root-Mean-Square Error $\langle e^2\rangle^{1/2}$ (m/s)	Third Moment $\langle e^3\rangle$, (m/s)^3	Skewness γ	Error Trend C_1, m/s
Brown	0.17	1.69	0.63	0.13	1.01
Smoothed Brown	−0.06	1.70	−2.21	−0.45	1.01
MCW	0.44	1.70	0.64	0.13	0.35
Equation (6)	−0.04	1.63	0.48	0.11	0.81
Equation (7) with (10)	0.01	1.70	−0.10	−0.02	0.43
Equations (7)–(9) and Figure 7	0.11	1.63	0.13	0.03	0.50
j-resolved	0.02	1.43	0.23	0.08	0.24

Notation is as follows: Error, e, of wind speed measurements by altimeter is defined as $e = U_S - U_B$. Angle brackets denote averaging over the data set. The skewness, γ, of the error distribution is $\langle e^3\rangle/\langle e^2\rangle^{3/2}$. The error trend is defined as the coefficient C_1 in the linear regression model: $e = C_0 + C_1\xi$ for the range $0 < \xi < 4$, and ξ is estimated on the basis of (3) using buoy data.

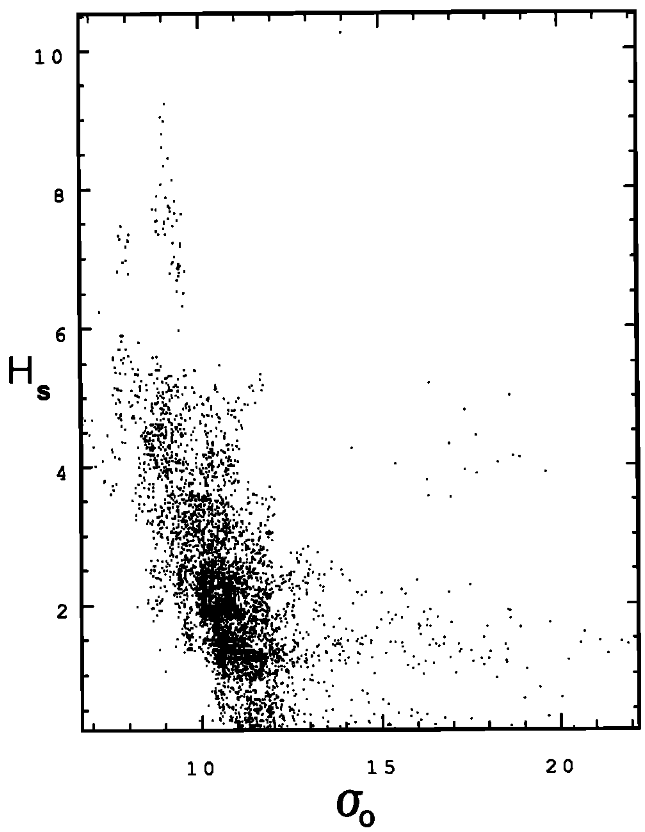

Fig. 2. Altimeter radar cross section σ_0 (decibels) and significant wave height H_S (meters), corrected using equation (4).

a GMF. This constraint concerns the smoothness of the model functions $U = f(\sigma_0)$ or $U = f(\sigma_0, H_S)$.

We compared the Brown GMF with the most recent GMF proposed by *Witter and Chelton* [1991]. The latter represents a modification of the Chelton-Wentz tabular GMF [*Chelton and Wentz*, 1986] and hence is called the modified Chelton-Wentz (MCW) function. When MCW was applied to our (unfiltered) data set, it was found to produce a very low wave age trend: $C_1 \approx 0.35$ m/s per unit ξ. This feature would make MCW highly useful for certain applications. Unfortunately, its other characteristics, as listed in Table 1, are less favorable: the mean bias, $\langle e \rangle = 0.44$ m/s, is considerably worse than that of the Brown GMF. In view of our earlier comments related to (1), we conclude that the original Brown GMF remains to be the best available algorithm by which to judge the progress in this field.

Apparently, in order to improve altimeter wind speed measurements in the sense of all the parameters employed in Table 1, it is not sufficient to use the radar cross section alone. As was mentioned earlier, the pseudo wave age ξ can be estimated based on H and U; and since ξ influences the radar cross section, an empirical GMF can be sought as a function of two variables

$$U = F(\sigma_0, H) \tag{5}$$

4. A CONTINUOUS GMF

Function (5) should be interpreted as a solution for U of the physically based relationship $\sigma_0 = f(U, \xi)$. The only known empirical attempt [*Monaldo and Dobson*, 1989] to derive (5) was inconclusive. We believe that the main obstacle here is a relatively low sensitivity of the radar cross section σ_0 to variations in ξ. As a result, random errors in H and σ_0 obscure the effects of wave age. The volume of the collocated Geosat/buoy observations employed by Monaldo and Dobson (236 data points) was too small, which further complicated the analysis.

Employing a much larger data set, we were able to derive a continuous function $F(\sigma_0, H)$ based on orthogonal Chebyshev polynomials $T_i(\tilde{H})$ and $T_j(\tilde{\sigma}_0)$:

$$U = \sum_{i=0}^{M} \sum_{j=0}^{N} C_{ij} T_i(\tilde{H}) T_j(\tilde{\sigma}_0) \tag{6}$$

in which the tilde over the variables H and σ_0 signifies that the SWH and radar cross section were normalized to vary within the interval $(-1, 1)$. The normalization rule is $\tilde{H} = [2H - (H_{max} + H_{min})]/(H_{max} - H_{min})$ and $\sigma_0 = [2\sigma_0 - (\sigma_{0max} + \sigma_{0min})]/(\sigma_{0max} - \sigma_{0min})$, where $H_{max} = 4.565$, $H_{min} = 1.118$, $\sigma_{0max} = 21.567$, and $\sigma_{0min} = 7.367$. Equation (6) rapidly loses its accuracy outside the "normal" range for σ_0 (which extends from 7.5 dB to 13.0 dB and covers more than 95% of all cases). For σ_0 outside this range, additional empirical dependencies had to be derived: at $\sigma_0 < 7.5$ a linear approximation is sufficient, $U = 43.559 - 3.443\sigma_0$, and at $\sigma_0 > 13$ dB the power law $U = 7.244 \times 10^6 \sigma_0^{-5.775}$ gives good results.

The empirical determination of the coefficients C_{ij} requires binning the values of one of the variables (we created six bins for the values of H). The distribution of data points in the σ_0-H plane is highly nonuniform (Figure 2), and the binning inevitably results in a considerable smoothing of the functional dependence. Consequently, some information on the influence of H becomes lost. Having tried various combinations of M and N in (6), we selected $M = 1$ and $N = 3$ as giving the best performance. In Table 2 the values of C_{ij} are provided as found using the NAG routine E02CA.

The (two-dimensional) Chebyshev polynomial expansion was chosen here for the same reasons for which it is used in many other engineering applications: fast convergence and wide availability as a standard routine in popular software packages.

The performance characteristics of the GMF (equation (6)) are given in Table 1. Evidently, this two-dimensional function represents a step forward with respect to the Brown GMF. However, in terms of the ξ-related error trend C_1 and the third moment $\langle e^3 \rangle$, this approach yields only a moderate improvement over the Brown GMF. The plot of this GMF for three values of H is given in Figure 3. The main advantages of (6) are a continuous dependence of the estimated wind speed on the altimeter SWH for at least 95% of all cases, a very low mean error $\langle e \rangle$, and a reduced rms error. The main drawback is the still significant ξ-related

TABLE 2. Coefficients C_{ij} in Equation (6)

	j			
i	0	1	2	3
0	30.50	−11.30	13.70	−0.763
1	2.64	4.49	2.72	2.44

error trend. An approach that decreases the error trend and the third moment even further is presented in the next section.

5. A CLASSIFIER-BASED GMF

The detrimental effect of the measurement noise in the variables σ_0 and H can be reduced by recognizing the fact that a continuous function approach is inherently flawed when one of the factors (SWH) has a relatively small influence on σ_0. Reviewing the physical mechanism responsible for the effect of ξ on the radar cross section [*Glazman*, 1990; *Glazman and Pilorz*, 1990], a classifier-based approach appears more promising. It is based on breaking all observations down into several subsets corresponding to different regimes in the sea surface's geometry (quantified by limited subranges of ξ), and then determining an individual relationship $U = F_\xi(\sigma_0)$ for each gradation. The wind speed dependence of the radar cross section will be different for such subsets, and this difference may be quite appreciable if the separation is done at properly selected boundaries. The simplest version of this approach is implemented by identifying just two subsets separated by a critical wave age, ξ_{cr}. According to our previous studies (see also Figure 1 of the present paper), the wave age dependence is rather weak for data points with $\xi \gtrsim 2$ and stronger for $\xi \lesssim 2$. Therefore it is natural to select ξ_{cr} near 2. Then in the first approximation, the effect of H could be taken into account as a factor influencing the separation of the data into the subsets. Since the wave age variability is much smaller within each subset than in the whole data set, we expect to obtain rather unambiguous relationships $U = F_\xi(\sigma_0)$ for these two groups.

Instead of using a sharp boundary, $\xi = \xi_{cr}$, we separated the data into two slightly overlapping subsets: subset 1 with $\xi < \xi_{cr} + \Delta\xi$ and subset 2 with $\xi > \xi_{cr} - \Delta\xi$. The values $\xi_{cr} = 1.89$ and $\Delta\xi = 0.03$ were found empirically as yielding the best endpoint results. Respectively, two empirical functions $F_j(\sigma_0)$ with $j = 1$ and 2, were derived. Each function is presented analytically by a set of smoothly merging curves.

For $j = 1$ this set consists of three curves:

TABLE 3. Coefficients in Equation (7)

j	$s_0^{(j)}$	$s_1^{(j)}$	$s_2^{(j)}$	$s_3^{(j)}$
1	−64.22	30.81	−3.63	0.13
2	106.58	−18.74	1.11	−0.02

If $\xi > \xi_{cr}$, $j = 2$. The units of U and σ_0 are meters per second and decibels, respectively.

$$U^{(1)} = 38.53 - 2.86\sigma_0 \qquad \sigma_0 < 7.5$$

$$U^{(1)} = \sum_{n=0}^{3} s_n^{(1)}\sigma_0^n \qquad 7.5 \le \sigma_0 \le 12.0 \tag{7}$$

$$U^{(1)} = 2.54 \times 10^3 \sigma_0^{-2.5} \qquad \sigma_0 > 12.0$$

For $j = 2$ this set consists of two curves:

$$U^{(2)} = \sum_{n=0}^{3} s_n^{(2)}\sigma_0^n \qquad \sigma_0 < 15.0$$

$$U^{(2)} = 24.18\sigma_0^{-0.96} \qquad \sigma_0 \ge 15.0 \tag{8}$$

For both $j = 1$ and $j = 2$, the cubic polynomials

$$U^{(j)} = \sum_{n=0}^{3} s_n^{(j)}\sigma_0^n \tag{9}$$

play the main role: more than 90% of all experimental points fall within the range of their applicability. The coefficients $s_n^{(j)}$ are summarized in Table 3. In Figure 4 the functions $F_j(\sigma_0)$ are plotted for both gradations j. As we expected, these functions are very different. Within their proper domains, they yield much more accurate estimates of the wind velocity than would be possible with a single function that ignores wave age gradations.

Assume for a moment that a crude information on the actual wave age is provided based on some independent measurements (for example, from a SAR). This information would help us select $j = 1$ or 2. With the value of j resolved,

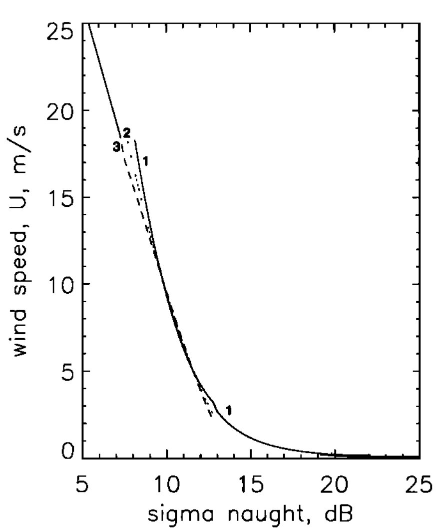

Fig. 3. Continuous GMF of section 4, for three values of SWH. Curve 1, $H_S = 0.5$ m; curve 2, $H_S = 3$ m; curve 3, $H_S = 6$ m.

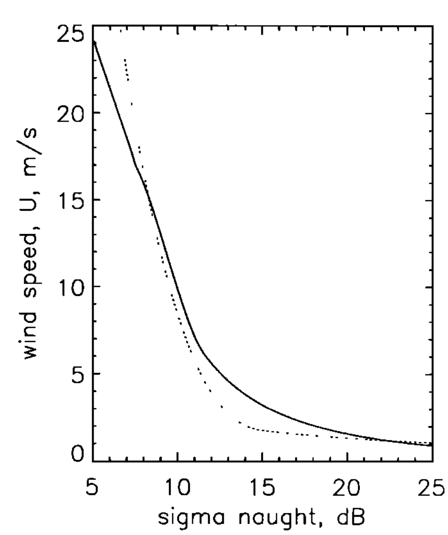

Fig. 4. Functions $U = F_j(\sigma_0)$ as specified by equations (7)–(9). Solid curve, $j = 1$; dashed curve, $j = 2$.

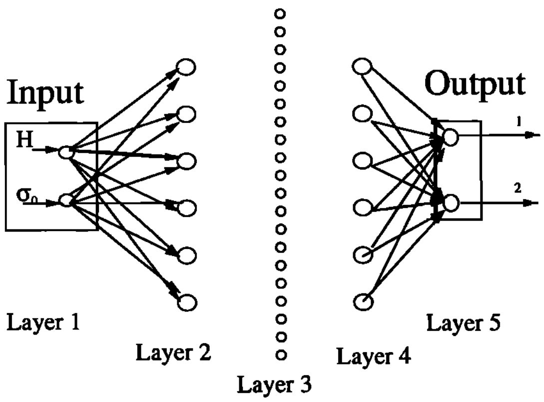

Fig. 5. Neural "feed forward" network (2-6-20-6-2) employed to develop a classifier (Figure 6) of the wave age gradations. Arrows illustrate the input-output flows (for external layers only). The endpoint output represents the value of j for equation (9). Each circle symbolizes the nonlinear transfer function ("sigmoid"), $g(u_k)$, which uses a weighted sum of input signals, $u_k = \sum w_{kn} v_n$, to produce its output. The "training" of the network consists in selecting the weights w_{kn} which yield the desirable output from the network.

equations (7)–(9) yield much more accurate estimates of the wind speed than does the Brown GMF. To test this model, we used the NDBC data to determine the actual wave age and thus resolve j, and then we estimated altimeter wind speed using (7)–(9). The rms error and other statistics of this algorithm are given in Table 1 as the "j-resolved" GMF.

In the absence of auxiliary information on the degree of wave development, determining the appropriate gradation of the wave age is a difficult problem. An empirical classifier which solves this problem is described in the next section.

6. Determination of the Wave Age Gradation Based on Altimeter Data

In Figure 2 the altimeter data are plotted as points on the plane $\sigma_0 - H$. Our task is to find the best empirical curve (demarcation line) dividing this plane into two regions: $j = 1$ with $\xi < \xi_{cr}$ and $j = 2$ with $\xi > \xi_{cr}$. Of course, such separation can be neither complete nor unambiguous, for the altimeter-supplied σ_0 and H yield at best only a crude estimate of the wave age; hence some points will be on the wrong side of the demarcation line. However, our GMF is partly protected from the identification failures because the curves $F_j(\sigma_0)$ (equations (7)–(9)) have been derived for slightly overlapping gradations of ξ (see section 5). In other words, for the points close to the demarcation line, either curve is more or less suitable. The problem exists mainly for the far away points, and it is those "bad" points which have the most adverse effect on the statistics of the wind speed error.

In order to determine the demarcation line, we used the entire set of σ_0, H_S values together with the buoy-reported pseudo wave age (equation (3)) and trained a simple (five layer) neural network (sketched in Figure 5) to select the correct gradation of ξ. Success of neural nets in selecting best candidates has been demonstrated by *Badran et al.* [1991] for the removal of directional ambiguity in scatterometer measurements of vector winds. A general introduction to this technique is given, for example, by *Lippmann* [1987]. The ability of neural nets to deal with highly correlated inputs is important for our application. Upon training, the neural network allowed us to plot a continuous function H_S versus σ_0 as shown in Figure 6. Ultimately (since neural networks are not easily transferable to other users), we approximated this function by a cubic polynomial

$$H = \sum_{i=0}^{3} b_i \sigma_0^i \tag{10}$$

using a least squares fit. The coefficients of the fit are b_i = [894.361, −244.596, 22.511, −0.696]. This procedure correctly identifies 83% of the data points; the points that are identified incorrectly are plotted in Figure 6. This classifier yielded excellent statistics of wind speed errors (see Table 1) including the wave-age-related trend. However, the rms error remained on the level of the Brown and MCW models.

The neural network approach brings us to two important conclusions: (1) a large majority of all points can be correctly resolved on the basis of SWH and σ_0, and (2) a general trend for the demarcation line $H(\sigma_0)$ is given by a decreasing function of σ_0.

Analyzing Figure 4, one can see that certain subranges of σ_0 have a greater adverse effect on wind error than other subranges. For example, misidentification of the points whose σ_0 is within 10 to 17 dB range results in greater wind speed errors (up to 2 m/s) than misidentification of other points (the errors are basically within 1 m/s). An exception to

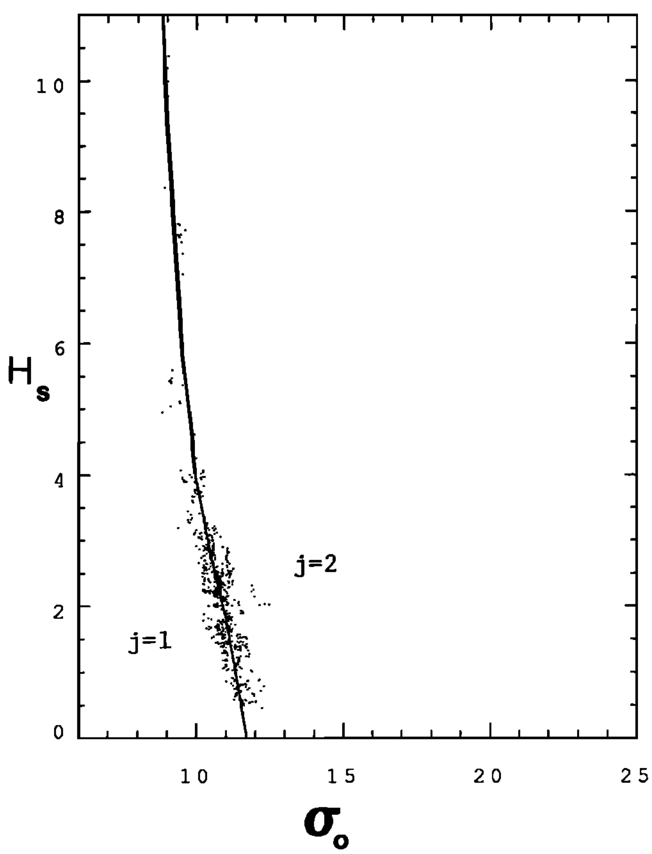

Fig. 6. The demarcation line drawn by the neural network. Points represent the subset of altimeter measurements from Figure 2 which have been incorrectly resolved by the neural network (17% of all cases).

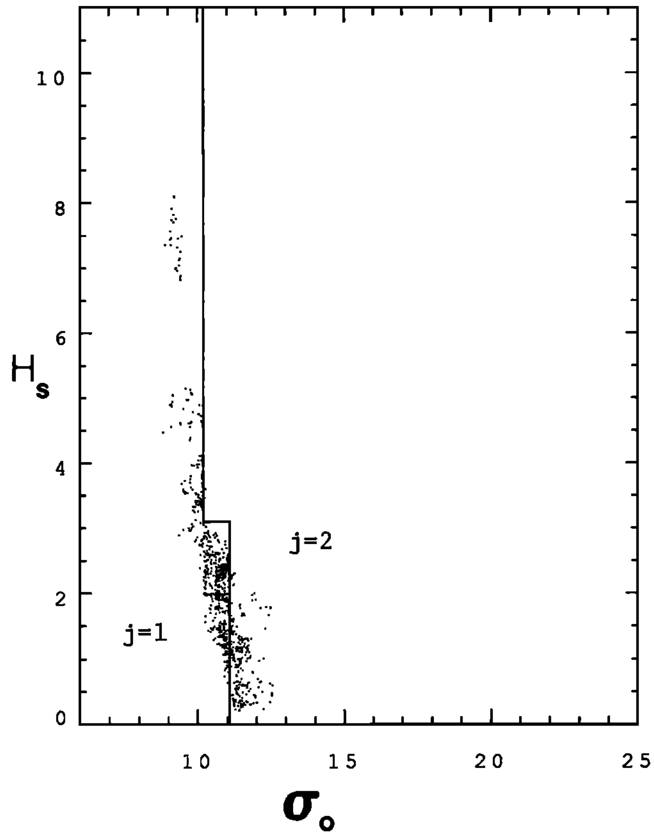

Fig. 7. The "optimal" classifier (see section 6 for detail). Coordinates of break points are as follows: for point A, H = 3.10 m, σ_0 = 10.25 dB, and for point B, H = 3.10 m, σ_0 = 11.05 dB. Points represent the subset of altimeter measurements from Figure 2 which have been incorrectly resolved by this identifier.

this rule is the range $\sigma_0 < 7.5$ dB. However, in this range almost all points belong to the low wave age gradation: hence a misidentification is extremely unlikely. This common-sense argument points at a possibility of deforming the demarcation curve so as to optimize certain desirable features of the GMF. Specifically, instead of requiring the absolute maximum number of correct identifications, we can demand only that the points resulting in larger wind speed errors be identified most effectively, while the points whose misidentification has little effect on the error can be ignored. This should reduce the rms error of the wind speed measurements and can be accomplished, for example, by selecting a sharp curve characterized by a small set of parameters, followed by varying these parameters until the desirable result is achieved. The procedure is empirical: we deform the curve and calculate the result (i.e., the rms error, etc.) after each deformation. The simplest such curve is a piecewise straight line shown in Figure 7. The coordinates of the break points, A and B, were taken as adjustable parameters (three independent numbers). Their "best" values are found as follows: point A, 3.10 m, 10.25 dB, and point B, 3.10 m, 11.05 dB. The resulting "optimal" classifier reduces the error trend (in terms of C_1) to an acceptable level of 0.5 m/s and keeps other error statistics within acceptable bounds, as shown in the fourth row of Table 1. The rms error is now reduced as compared to the classifier (10). However, as is discussed in section 7, this classifier has a drawback that may have an adverse effect in certain applications.

The choice of a classifier should be based on specific requirements for the problem at hand. Evidently, the "neural net" classifier appears most advantageous for climate studies and global circulation modeling, in which the wave-age-related error trend, the mean error bias $\langle e \rangle$, and the error skewness $\langle e^3 \rangle$ must all be small. If, however, the rms error is of predominant importance (which may be the case when the data available for taking averages are limited), the "optimal" classifier has an advantage.

7. WIND SPEED HISTOGRAMS

The goal of the present work was to increase the accuracy of wind speed determination for individual measurements. We sought to minimize the rms error of the wind speed algorithm and, additionally, introduced two more constraints on the measuring error. However, in some oceanographic applications, the accuracy of individual measurements in terms of the rms error is not important. For instance, for studies of wind speed statistics (for an ocean region or season, etc.), the only feature required for a GMF is its ability to minimize the mean error $\langle e \rangle$ within the desired wind speed gradations.

It has been noted [*Dobson et al.*, 1987] that the Brown algorithm [*Brown et al.*, 1981], regardless of its low rms error, results in distortions of wind speed histograms if the wind speed gradations are narrow. This happens because the Brown GMF includes three curves $U = f(\sigma_0)$ matching at σ_0 = 10.12 and σ_0 = 10.9 dB and yielding a discontinuous derivative $dU/d\sigma_0$ at the junctions. The discontinuity yields singularities (spikes) in the probability density function. To rectify the problem, a "smoothed Brown" GMF was suggested in the form of a fifth-degree polynomial, $U = \sum a_n \sigma_0^n$, which approximates the original Brown algorithm [*Dobson et al.*, 1987] in the range 8 dB < σ_0 < 15 dB. Within the corresponding wind speed interval, 1.54 to 15 m/s, the smoothed GMF is claimed to have an advantage over the original Brown GMF because it yields unimodal wind histograms, whereas the original Brown GMF may produce false peaks.

Actually, all presently available GMFs yield singularities at some point (or points) and distort the histograms to a greater or lower degree. The Brown smooth GMF, if extended beyond the range 1.54–15 m/s, may yield singularities at the junctions. The MCW function discussed in section 3 has singularities at all points for which it is given in the tabular form because this GMF involves a linear interpolation between the points; hence it has discontinuous $d\sigma_0/dU$ at each such point. The GMFs developed in the present work would also yield singularities: the "continuous" GMF of section 4 yields singularities at points σ_0 = 7.5 dB and σ_0 = 13 dB, while the "optimal classifier" of section 6 would yield singularities at points σ_0 =10.25 dB and σ_0 = 11.05 dB (because the line in Figure 7 is not differentiable). The "neural net" classifier approximated by (10) also distorts the probability distribution because it involves branching. Hence the question arises as to whether and how one should use these algorithms for wind speed statistics.

The short answer is that all algorithms mentioned above, including the original Brown and the tabular GMFs, can be used in statistical problems. However, the choice of a

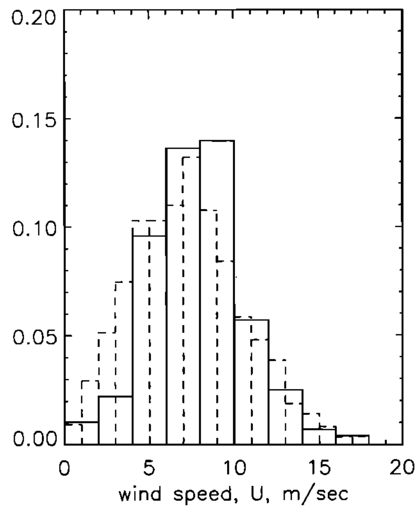

Fig. 8. Histograms of wind speed distributions. Solid line histograms represent altimeter wind speeds obtained with the original Brown algorithm; the gradation width is set to 2 m/s. Dashed histograms show wind speeds measured by NDBC buoys; the gradation width is set to 1 m/s. The vertical axis represents relative frequency.

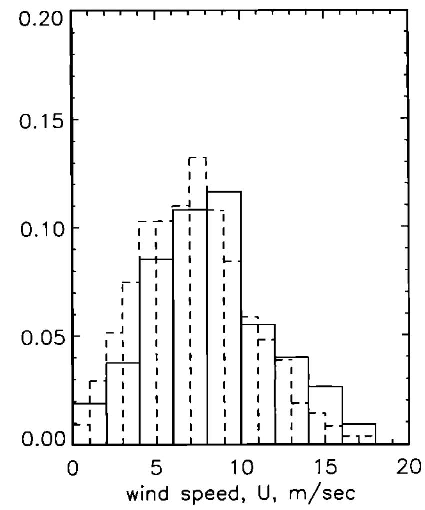

Fig. 10. The same as Figure 8, except that solid histograms represent the modified Chelton-Wentz GMF.

specific GMF depends on the problem at hand. If the wind speed gradations were arbitrarily narrow, a GMF would have to possess continuous derivatives. However, in practice, the gradations have finite width. Hence by an appropriate adjustment of wind speed gradations, the impact of singularities and branching can be controlled or eliminated. To illustrate this point, we present wind speed distributions for our collocated measurements, using wind gradations 2 m/s wide. The original Brown, Smoothed Brown, modified Chelton-Wentz, and classifier-based (equation (10)) GMFs are illustrated in Figures 8, 9, 10, and 11. Evidently, all four GMFs disagree with the "ground truth" histogram in some ranges. However, the Brown smooth GMF is definitely not the best to use for wind speed statistics.

8. CONCLUSIONS

Actual wave dynamics and surface roughness regimes are highly diverse and are much more complex than those implied in our preceding theoretical analyses [*Glazman and Weichman*, 1989; *Glazman*, 1990; *Glazman and Srokosz*, 1991]. However, the success of the present experimental effort indicates that the idealized notion of the degree of sea development (quantified by the pseudo wave age) is a viable concept which remains practically useful under realistic conditions. The present work, in particular the "j-resolved" algorithm analyzed in the bottom row of Table 1, also indicates that there exists a potential for further improvement of the accuracy of altimeter measurements.

The increased accuracy of the wind speed determination achieved by the wave-age-dependent algorithms makes it theoretically possible to further improve estimates of the sea state bias for sea level measurements, for example following the procedure suggested by *Fu and Glazman* [1991].

The use of only two gradations of the wave age (sections 5 and 6) was dictated here by the relatively small number of

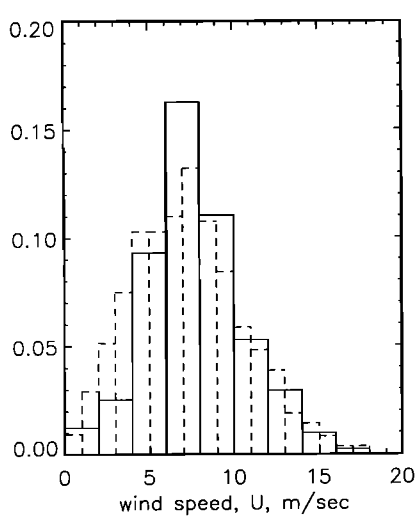

Fig. 9. The same as Figure 8, except that solid histograms represent the smoothed Brown GMF.

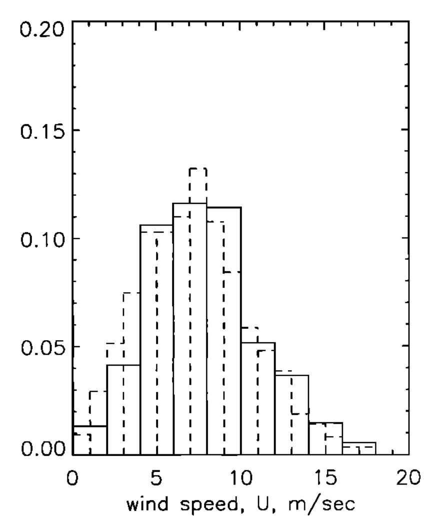

Fig. 11. The same as Figure 8, except that solid histograms represent the classifier-based GMF using equation (10).

data available for analysis. New satellite missions, ERS-1 and TOPEX, will eventually yield more accurate and voluminous data, which will permit a more detailed stratification of the wave age gradations, leading to more accurate wind speed and sea state bias algorithms.

The classifier-based GMFs can be successfully used for constructing histograms of wind speed distribution. However, we recommend that the width of wind speed gradations for such analyses be greater than 1 m/s.

Acknowledgments. This work was performed at the Jet Propulsion Laboratory, California Institute of Technology, under contract with the National Aeronautics and Space Administration.

REFERENCES

Badran, F., S. Thiria, and M. Crepon, Wind ambiguity removal by the use of neural network techniques, *J. Geophys. Res.*, *96*(C11), 20,521–20,529, 1991.

Brown, G. S., H. R. Stanley, and N. A. Roy, The wind speed measurement capability of spaceborne radar altimeters, *IEEE J. Oceanic Eng.*, *OE-6*(2), 59–63, 1981.

Carter, D. J. T., P. G. Challenor, and M. A. Srokosz, An assessment of Geosat wave height and wind speed measurements, *J. Geophys. Res.*, *97*(C7), 11,383–11,392, 1992.

Chelton, D. B., and F. J. Wentz, Further development of an improved altimeter wind speed algorithm, *J. Geophys. Res.*, *91*(C12), 14,250–14,260, 1986.

Dobson, E. B., F. M. Monaldo, J. Goldhirsh, and J. Wilkerson, Validation of Geosat altimeter-derived wind speeds and significant wave heights using buoy data, *J. Geophys. Res.*, *92*(C10), 10,719–10,731, 1987.

Fu, L.-L., and R. E. Glazman, The effect of the degree of wave development on the sea-state bias in radar altimetry measurements, *J. Geophys. Res.*, *96*(C1), 829–834, 1991.

Gilhousen, D. B., A field evaluation of NDBC moored buoy winds, *J. Atmos. Oceanic Technol.*, *4*(1), 94–104, 1987.

Glazman, R. E., Near-nadir radar backscatter from a well-developed sea, *Radio Sci.*, *25*(6), 1211–1219, 1990.

Glazman, R. E., Statistical problems of wind-generated gravity waves arising in microwave remote sensing of surface winds, *IEEE Trans. Geosci. Remote Sens.*, *29*(1), 135–142, 1991*a*.

Glazman, R. E., Reply, *J. Geophys. Res.*, *96*(C3), 4979–4983, 1991*b*.

Glazman, R. E., and S. H. Pilorz, Effects of sea maturity on satellite altimeter measurements, *J. Geophys. Res.*, *95*(C3), 2857–2870, 1990.

Glazman, R. E., and M. A. Srokosz, Equilibrium wave spectrum and sea state bias in satellite altimetry, *J. Phys. Oceanogr.*, *21*(11), 1609–1621, 1991.

Glazman, R. E., and P. Weichman, Statistical geometry of a small surface patch in a developed sea, *J. Geophys. Res.*, *94*(C4), 4998–5010, 1989.

Lippmann, R. P., An introduction to computing with neural nets, *IEEE Trans. Acoust. Speech Signal Process.*, *4*, 4–22, 1987.

Monaldo, F., and E. Dobson, On using significant wave height and radar cross section to improve radar altimeter measurements of wind speed, *J. Geophys. Res.*, *94*(C9), 12,669–12,701, 1989.

Pierson, W. J., Comment on "Effects of sea maturity on satellite altimeter measurements" by R. E. Glazman and S. H. Pilorz, *J. Geophys. Res.*, *96*(C3), 4973–4977, 1991.

Witter, D. L., and D. B. Chelton, A Geosat altimeter wind speed algorithm and a method for altimeter wind speed algorithm development, *J. Geophys. Res.*, *96*(C5), 8853–8860, 1991.

R. E. Glazman and A. Greysukh, Jet Propulsion Laboratory, California Institute of Technology, 4800 Oak Grove Drive, Pasadena, CA 91109.

(Received May 27, 1992;
revised November 5, 1992;
accepted November 5, 1992.)